AIAA JOURNAL
Vol. 40, No. 1, January 2002

Response and Failure Characteristics of Internally Pressurized Elliptical Composite Cylinders

Jennifer M. McMurray* and Michael W. Hyer†
Virginia Polytechnic Institute and State University, Blacksburg, Virginia 24061

The characteristics of the response of internally pressurized thin-walled elliptical composite cylinders, including failure, are discussed. The influence of the elliptical geometry on response is illustrated by comparison with a circular cylinder. It is shown that with internal pressure elliptical cylinders tend to become more circular by exhibiting inward normal displacements at some circumferential locations and by the existence of circumferential displacements. The influence of material orthotropy is illustrated by considering axially stiff, circumferentially stiff, and quasi-isotropic laminates. The results show that orthotropy can be used to counter the influence of the circumferentially varying curvature by producing circumferential strains at the midcylinder axial location of a circumferentially stiff cylinder that are almost independent of the circumferential coordinate, much like the axisymmetric response of a circular cylinder. The influence of geometric nonlinearities is studied by inclusion of the von Kármán terms in the strain-displacement relations, and it is shown that one of the primary effects is flattening of the ellipse in the regions near the ends of the minor diameter. Because of varying curvature in the circumferential direction, there can be, effectively, a stress concentration at certain circumferential locations, which are sites of failure initiation, the exact location depending on material orthoropy. To study failure initiation, two failure criteria are considered: the interactive Hashin criterion and the noninteractive maximum stress criterion. These criteria are used to compute the pressures to cause first matrix cracking and first fiber failure. It is demonstrated that the predictions of the two criteria are not that different, and the pressure to cause first fiber failure is about twice the pressure to cause first matrix failure. Additionally, it is shown that matrix cracking begins in the circumferentially stiff cylinder at lower pressures than in the axially stiff and quasi-isotropic cylinders, and the location of failure is different.

Background

CYLINDERS are often used as the idealized model for a number of important structures. Aircraft fuselages, missile cases, submarine hulls, and tankage for storing and transporting various liquids and gases are but a few examples. Circular cylindrical cross sections are generally used as the basis for many of the models, and much has been written regarding the analysis of circular cylinders. However, future aircraft fuselage designs can depart substantially from the normal circular cross section, and future reusable launch vehicles can use fuel tanks that are noncircular. Aerodynamic, structural, or payload considerations can dictate the noncircular designs. These aerospace structures can also be idealized as cylinders, but with noncircular cross sections. Because fiber-reinforced composite materials are often the material of choice for aerospace applications, because of weight and design flexibility, it is logical to consider composite materials for fuselage and fuel tank applications. In both cases failure in the sense of catastrophic material failure is important, but also, failure in the sense of leakage of the cylinder wall as a result of matrix cracking can be important. This paper examines the failure of internally pressurized noncircular cylinders by considering cylinders of elliptical cross section. Failure is addressed by using a first-ply failure approach. Although first-ply failure analysis does not imply catastrophic material failure or leakage problems, a study of failure at this level does bring to light the influence of noncircular geometry and material orthotropy on the general response of composite cylinders and, in particular, the influence on stresses. Additionally, because an in-depth study of failure of composite cylinders where a significant percentage of the fibers have failed must consider a progressive failure analysis, a study of failure at this initial level is an important stepping stone for more advanced failure analyses. Elliptical cross sections are considered because analytical expressions can be written to represent the geometry of the cross section. It is felt that many of the conclusions reached for the case of elliptical cross sections also hold for more general noncircular cross sections. A recent survey by Soldatos[1] cataloged past work in the area of noncircular cylinders. There is no need to reiterate that review here except to say that work in the area of failure of noncircular composite cylinders is practically nonexistent.

The sections that follow define the specific problem being addressed. The geometry, boundary conditions, and general nomenclature are introduced. The semi-closed-form solution used to obtain numerical results is outlined. The character of the response of an internally pressurized elliptical cross-section cylinder is discussed. Then, the use of two failure criteria to predict first matrix failure and first fiber failure is described. One criterion is an interactive criterion, and the other is noninteractive. The pressure level, mode, and location of failure for each criterion are determined and compared. Finally, an alternative view of the failure analysis is considered.

Problem Description

The problem considered consists of the cylinder described in Fig. 1, with $2a$, $2b$, and L denoting, respectively, the major diameter, minor diameter, and length of the cylinder reference surface. The degree of ellipticity e is defined here as the ratio b/a, and C defines the circumference of the reference surface. The wall thickness of the cylinder, which is assumed to be thin walled, is denoted by H and the internal pressure by p_o. The displacement of the reference surface in the axial x direction is denoted by $u^o(x, s)$, that in the circumferential s direction by $v^o(x, s)$, and that in the direction normal to the reference surface by $w^o(x, s)$. Transverse shear deformations are ignored. The upper part of the cross section is referred to as the crown, the lower part as the keel, and the sides as the sides. It will be assumed that the cylinder ends are clamped to a rigid end plate or bulkhead, which can move axially. Accordingly, clamped boundary conditions are applied to each end of the cylinder, with the exception of allowing the end at $x = +L/2$ to translate uniformly in the axial

Presented as Paper 2000-1516 at the 41st Structures, Structural Dynamics, and Materials Conference, Atlanta, GA, 3–6 April 2000; received 7 August 2000; revision received 10 May 2001; accepted for publication 1 June 2001.

*Graduate Research Associate, Department of Engineering Science and Mechanics; jmcmurra@vt.edu.

†Professor, Department of Engineering Science and Mechanics; hyerm@vt.edu. Associate Fellow AIAA.

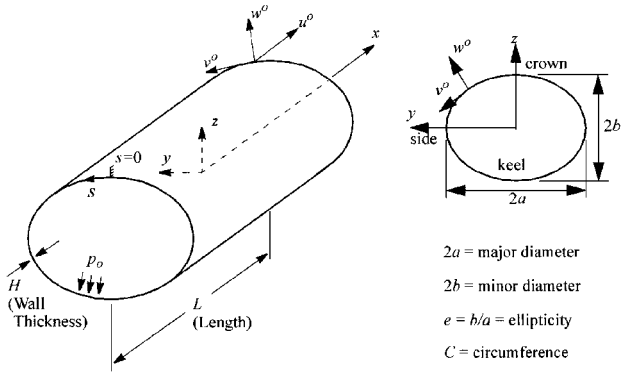

Fig. 1 Problem description, nomenclature, and geometry of an elliptical cylinder.

direction with displacement Δ. The end at $x = -L/2$ cannot move axially in order to restrict axial rigid-body translation. Formally, the boundary conditions at the ends of the cylinder ($x = \pm L/2$) are

$$u^o = 0 \;@\; x = -\frac{L}{2}, \qquad u^o = \Delta \;@\; x = +\frac{L}{2} \tag{1a}$$

$$v^o = 0 \tag{1b}$$

$$w^o = 0 \tag{1c}$$

$$\frac{\partial w^o}{\partial x} = 0 \tag{1d}$$

The end displacement Δ is determined by enforcing axial equilibrium of the end enclosure at $x = +L/2$, namely,

$$\int_0^C N_x \, \mathrm{d}s = p_o \pi a b \tag{2}$$

where N_x is the axial force resultant within the cylinder (to be defined shortly) and the cross-sectional area of the ellipse is πab. Physically, Eq. (2) states that the net axial force caused by the internal pressure times the cross-sectional area of the end enclosure must be balanced by the net axial force caused by the axial force resultant. These boundary conditions correspond to those that will be experienced by planned experiments with small-scale cylinders. The ends are to be potted into grooves in thick endplates.

Solution Approach

The solution procedure begins with the expression for the total potential energy of the cylinder, namely,

$$\pi = \frac{1}{2}\int_0^C \int_0^L \left[N_x \varepsilon_x^o + N_s \varepsilon_s^o + N_{xs}\gamma_{xs}^o + M_x \kappa_x^o + M_s \kappa_s^o + M_{xs}\kappa_{xs}^o - p_o w^o\right] \mathrm{d}x \, \mathrm{d}s \tag{3}$$

The pressure loading does not change directions with cylinder deformation. The force and moment resultants in Eq. (3) are defined by

$$N_x = \int_{-H/2}^{H/2} \sigma_x \, \mathrm{d}\zeta = A_{11}\varepsilon_x^o + A_{12}\varepsilon_s^o$$

$$M_x = \int_{-H/2}^{H/2} \sigma_x \zeta \, \mathrm{d}\zeta = D_{11}\kappa_x^o + D_{12}\kappa_s^o + D_{16}\kappa_{xs}^o$$

$$N_s = \int_{-H/2}^{H/2} \sigma_s \, \mathrm{d}\zeta = A_{12}\varepsilon_x^o + A_{22}\varepsilon_s^o$$

$$M_s = \int_{-H/2}^{H/2} \sigma_s \zeta \, \mathrm{d}\zeta = D_{12}\kappa_x^o + D_{22}\kappa_s^o + D_{26}\kappa_{xs}^o$$

$$N_{xs} = \int_{-H/2}^{H/2} \tau_{xs} \, \mathrm{d}\zeta = A_{66}\gamma_{xs}^o$$

$$M_{xs} = \int_{-H/2}^{H/2} \tau_{xs} \zeta \, \mathrm{d}\zeta = D_{16}\kappa_x^o + D_{26}\kappa_s^o + D_{66}\kappa_{xs}^o \tag{4}$$

where ζ is the through-thickness coordinate within the cylinder wall. As seen from the form of Eq. (4), only symmetric and balanced laminates are being considered. The reference surface strains and curvatures in the energy expression are related to the reference surface displacements by

$$\varepsilon_x^o = \frac{\partial u^o}{\partial x} + \underline{\frac{1}{2}\left(\frac{\partial w^o}{\partial x}\right)^2}, \qquad \varepsilon_s^o = \frac{\partial v^o}{\partial s} + \frac{w^o}{R(s)} + \underline{\frac{1}{2}\left(\frac{\partial w^o}{\partial s}\right)^2}$$

$$\gamma_{xs}^o = \frac{\partial u^o}{\partial s} + \frac{\partial v^o}{\partial x} + \underline{\left(\frac{\partial w^o}{\partial x}\right)\left(\frac{\partial w^o}{\partial s}\right)}, \qquad \kappa_x^o = -\frac{\partial^2 w^o}{\partial x^2}$$

$$\kappa_s^o = -\frac{\partial^2 w^o}{\partial s^2}, \qquad \kappa_{xs}^o = -2\frac{\partial^2 w^o}{\partial x \partial s} \tag{5}$$

Note that the radius of curvature being a function of s in ε_s^o is what makes this problem different than that of a circular cylinder and the Donnell shell theory is being used. The underlined terms in Eq. (5) denote the geometric nonlinearities considered. These are the von Kármán approximations to the fully nonlinear strain-displacement relations that are included here when the effects of geometric nonlinearities are to be considered. Donnell shell theory is felt to be adaquate compared to, for example, Sanders's theory, because the circumferential displacement term in Sanders's theory $v^o(x, s)/R$ is expected to be outweighted by the circumferential gradient of the normal displacement, and the gradients of the inplane displacements are not expected to be excessive.

With the radius of curvature varying circumferentially, a closed-form solution to the problem is not easily found. Accordingly, an approximate solution is sought, and here one where the role of the important material and geometric parameters in the problem can be indentified further into the analysis is than with, say, a purely numerical approach. To begin the approximate solution, the circumferential variation of the inverse radius of curvature is expanded, in a method suggested by Marguerre[2] in a cosine series, such that

$$\frac{1}{R(s)} \cong \sum_{i=0}^{I} a_{4i} \cos\frac{4i\pi s}{C} \tag{6}$$

where the coefficients a_{4i} are constants, which depend on the specific cross-sectional geometry (diameters $2a$ and $2b$) and I is the number of terms needed to properly represent the variation of the inverse radius of curvature. In conjunction with the Kantorovich method, the dependence of the reference surface displacements on the circumferential coordinate is approximated by a harmonic series using a form inspired by the inverse radius of curvature, namely,

$$u^o(x, s) = u_o^o(x) + \sum_{n=1}^{N} u_n^o(x) \cos\frac{4n\pi s}{C} + \sum_{m=1}^{M} u_{N+m}^o(x) \sin\frac{4m\pi s}{C}$$

$$v^o(x, s) = v_o^o(x) + \sum_{m=1}^{M} v_m^o(x) \cos\frac{4m\pi s}{C} + \sum_{n=1}^{N} v_{M+n}^o(x) \sin\frac{4n\pi s}{C}$$

$$w^o(x, s) = w_o^o(x) + \sum_{n=1}^{N} w_n^o(x) \cos\frac{4n\pi s}{C} + \sum_{m=1}^{M} w_{N+m}^o(x) \sin\frac{4m\pi s}{C} \tag{7}$$

where M and N determine the number of terms in the various series. For an isotropic elliptical cylinder, sine terms would not be necessary for $u^o(x, s)$ and $w^o(x, s)$, whereas cosine terms would not be necessary for $v^o(x, s)$. The presence of the bending stiffness terms D_{16} and D_{26} makes inclusion of these terms necessary.

Substituting the displacements of Eq. (7) into the strains and curvatures of Eq. (5), and these, in turn, into the stress and moment resultants of Eq. (4), integration of the energy expression with respect to s can be performed explicitly. The integrand of the energy expression is then dependent on the coefficients in Eq. (7), which

are only a function of x. As a result, the energy expression can be written symbolically as

$$\pi = \int_{-L/2}^{+L/2}\left[\int_0^C U(x,s)\,\mathrm{d}s\right]\mathrm{d}x = \int_{-L/2}^{+L/2} F[y_i(x),\, y_i'(x),\, y_i''(x)]\,\mathrm{d}x \qquad [i = 1, 3(N+M+1)] \quad (8)$$

In Eq. (8) the $y_i(x)$ represent the functional coefficients in Eq. (7), and $(\,)'$ represents differentiation with respect to the axial coordinate x. Although the integrand in Eq. (8) is also a function of cylinder geometry, material properties, and the pressure, these quantities are constants that would not be involved in a variational process. Accordingly, equating the first variation of the total potential energy to zero results in the Euler–Lagrange equations for the $y_i(x)$ and the associated variationally consistent boundary conditions at $x = \pm L/2$. The boundary conditions of Eq. (1) translate into specifying values of $y_i(x)$ and $y_i'(x)$ at $x = \pm L/2$. Defining intermediate variables in order to reduce the system to first-order form, it is possible to obtain a set of coupled nonlinear first-order ordinary differential equations, which are integrated by the finite difference method using the International Math and Statistical Library (IMSL) subroutine DBVPFD,[3] a variable-order, variable-step-size algorithm employing Newton's method. By rendering the governing Euler–Lagrange equations to first-order form, various derivatives of u^o, v^o, and w^o are directly available for computing reference surface strains and curvatures and force and moment resultants. More importantly, stresses as a function of x, s, and ζ can be computed. It has been found that using $I = 7$ in Eq. (6) and $N = 7$, $M = 4$ in Eq. (7) yields satisfactory results. More about the solution scheme and its accuracy can be found in Ref. 4.

Character of the Response

Though ultimate interest with elliptical cylinders is for application to aircraft fuselage structures and reusable launch vehicles, initial experimental work will take place in the laboratory with small-scale cylinders. The displacement, strain, and stress response of these smaller cylinders must be understood before studies of large-scale cylinders can commence. To that end, in the present study numerical results will be shown for eight- and nine-layer graphite-epoxy cylinders with major diameters of 0.254 m, ellipticities of 0.7, and lengths of 0.318 m. The material and geometric properties of a layer of graphite epoxy are taken to be

$$E_1 = 130.0\ \text{GPa}, \qquad E_2 = 9.70\ \text{GPa}, \qquad G_{12} = 5.00\ \text{GPa}$$
$$\upsilon_{12} = 0.300, \qquad h = 0.1400\ \text{mm} \quad (9)$$

where h is the thickness of a single layer. The laminates considered are quasi isotropic, $[\pm 45/0/90]_S$; axially stiff, $[\pm 45/0_2/90_{1/2}]_S$; circumferentially stiff, $[\pm 45/90_2/0_{1/2}]_S$, where 0 deg is the axial direction. These layups were selected because each has at least one layer with its fibers in the axial direction, at least one layer with its fibers in the circumferential direction, and ±45-deg layers. Eight or nine layers is a reasonable number from the point of view of manufacturing the small-scale cylinders by hand on elliptical mandrels. The study of one value of ellipticity is perhap limiting, but it is all that is necessary to demonstate the influence of elliptical geometry relative to a circular geometry. For that purpose the axial, circumferential, and normal displacement responses of an elliptical cylinder subjected to internal pressure can be contrasted with those of a circular cylinder by referring to Fig. 2. For this comparison the quasi-isotropic laminate is chosen, and a geometrically linear analysis is used. The displacements have been nondimensionalized by the laminate thickness H. An internal pressure of $p_o = 0.690$ MPa is used to compute the results. The format of the Fig. 2 illustrates the response of one-eighth of the cylinder. The coordinate locations have been normalized, and, referring to Fig. 1, the range of $0 \le x/L \le 0.5$ and $0 \le s/C \le 0.25$ is considered. Because of the presence of D_{16} and D_{26}, the problem does not exhibit octant symmetry. However looking at only one-eighth of the cylinder provides a fairly accurate detail of the response and simplifies displaying the results. Implementing symmetry and antisymmetry arguments for various responses, the response for the remainder of the cylinder can be envisioned.

Regarding the axial displacement, for an internally pressurized circular cylinder the axial displacement would be the net result of the pressure forcing the end enclosures apart and the Poisson effect caused by circumferential expansion pulling them together. Because for a circular cylinder the problem is axisymmetric, the result is an axial displacement that varies in near-linear fashion with the axial coordinate independent of s. Recall from the boundary conditions of Eq. (1) that the axial displacement would be zero at $x/L = -0.5$. At $x/L = +0.5$ the axial displacement would be determined by Eq. (2). Because of the nearly linear variation with x for the circular case, the axial displacement at $x/L = +0.5$ would be approximately twice the value at $x/L = 0$. As seen in Fig. 2, for the elliptical cylinder the axial displacement response is not axisymmetric and is far from being linear with x. Along the crown of the elliptical cylinder $s/C = 0$, the axial displacement is positive, while along the side $s/C = 0.25$ the axial displacement is actually negative at certain axial locations. Because the axial displacement changes signs with spatial location, there are some locations besides $x/L = -0.5$, where the axial displacement is zero. The axial displacement at $x/L = 0$ is

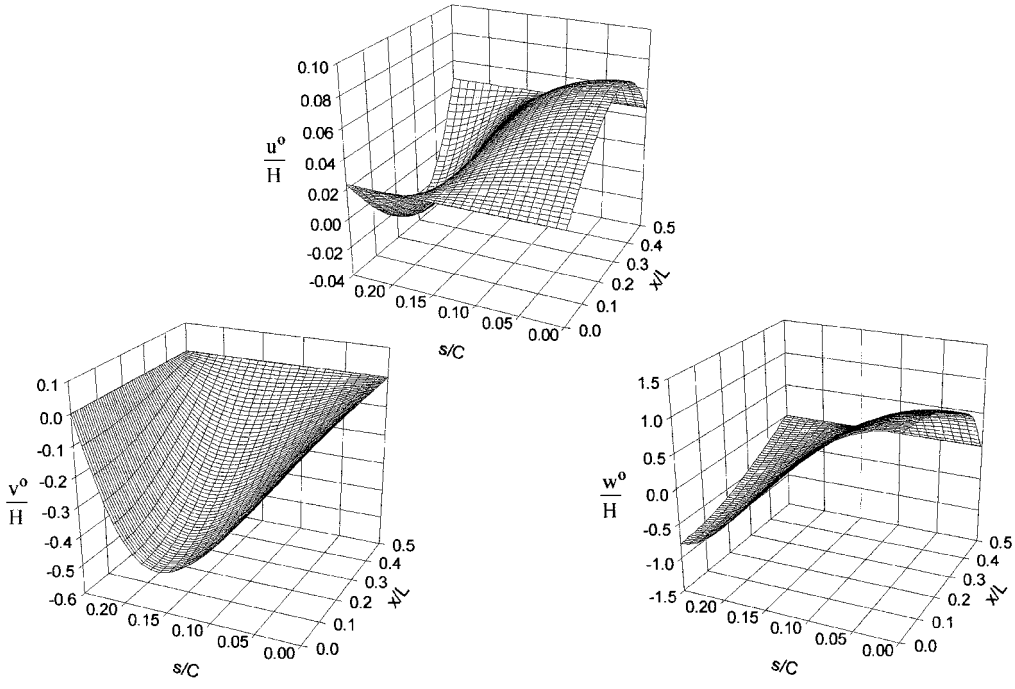

Fig. 2 Effect of elliptical geometry on the displacements.

practically independent of s, as it is at $x/L = +0.5$, and the axial displacements at these two locations differ by a factor of two, as they would for the circular case.

For balanced symmetric laminates an internally pressurized circular cylinder has no circumferential displacement response. However, as shown in Fig. 2 the elliptical case shows circumferential movement away from the sides and toward the crown and keel of the cylinder, a response that clearly distinguishes an elliptical cylinder from a circular one and one that has consequences at the ends of the cylinder where displacements are constrained to be zero. The existence of circumferential displacements also has consequences if circumferential stiffeners are used, as the cylinder wall would tend to shear in the circumferential direction relative to the stiffener. Figure 2 illustrates another distinguishing difference between circular and elliptical cylinders. With internal pressure the normal displacement of a circular cylinder would be outward everywhere. In contrast, under internal pressure the elliptical cylinder moves outward at the crown and keel, but moves inward at the sides. The cylinder tends to become more circular. This also has important consequences at the ends of the cylinder and would have consequences in the presense of circumferential stiffeners.

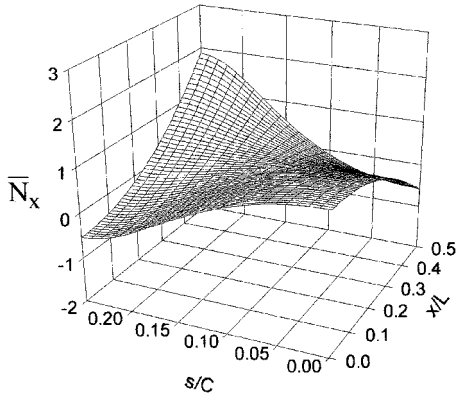

Fig. 3 Effect of elliptical geometry on the axial force resultant.

The spatial variations of the three components of displacement lead to strains, curvatures, and force and moment resultants that vary with circumferential, as well as axial, location. For example, the axial force resultant, shown in nondimensional form in Fig. 3 for the quasi-isotropic case, is compressive at certain circumferential locations, much as the axial displacement is. This behavior is not what would be expected in the presence of internal pressure. In. Fig. 3 the nondimensional axial force resultant $\bar{N}_x$ is the axial force resultant divided by $p_o a$.

To demonstrate the influence of orthotropy, or lamination sequence, the normalized circumferential reference surface strain $\bar{\varepsilon}_s^o$ is considered. Here the strains are normalized by the circumferential strains that would occur in a circular quasi-isotropic cylinder of diameter $2a$ subjected to the same pressure. As seen in Fig. 4, particularly the upper-left subfigure, the degree to which the circumferential strain varies with the s coordinate at the midspan is determined in large part by the laminate considered. As is well known, the circumferential strain for a circular cylinder has no variation with the s coordinate, independent of lamination sequence. Figure 4 suggests that at midspan the circumferentially stiff laminate mitigates, to a certain degree, the effect of ellipticity, as the strain does not vary as much with s there as it does with the other two laminates. Specifically, the circumferential strain varies by 58% around the circumference for the axially stiff case, by 44% for the quasi-isotropic case, and by 30% for the circumferentially stiff case. Therefore, it appears that the percentage of fibers in the circumferential direction in an elliptical cylinder controls the degree of variation with s of the circumferential strain at midspan. This suggests that allowing the character of material orthoropy to vary with circumferential position, i.e., allowing the fiber angles to vary with circumferential position, can provide a means to counter the influence of the curvature varying with circumferential position.

To demonstrate the influence of geometric nonlinearities, nondimensionalized circumferential curvature for the quasi-isotropic case is considered. The differences between linear and nonlinear analyses

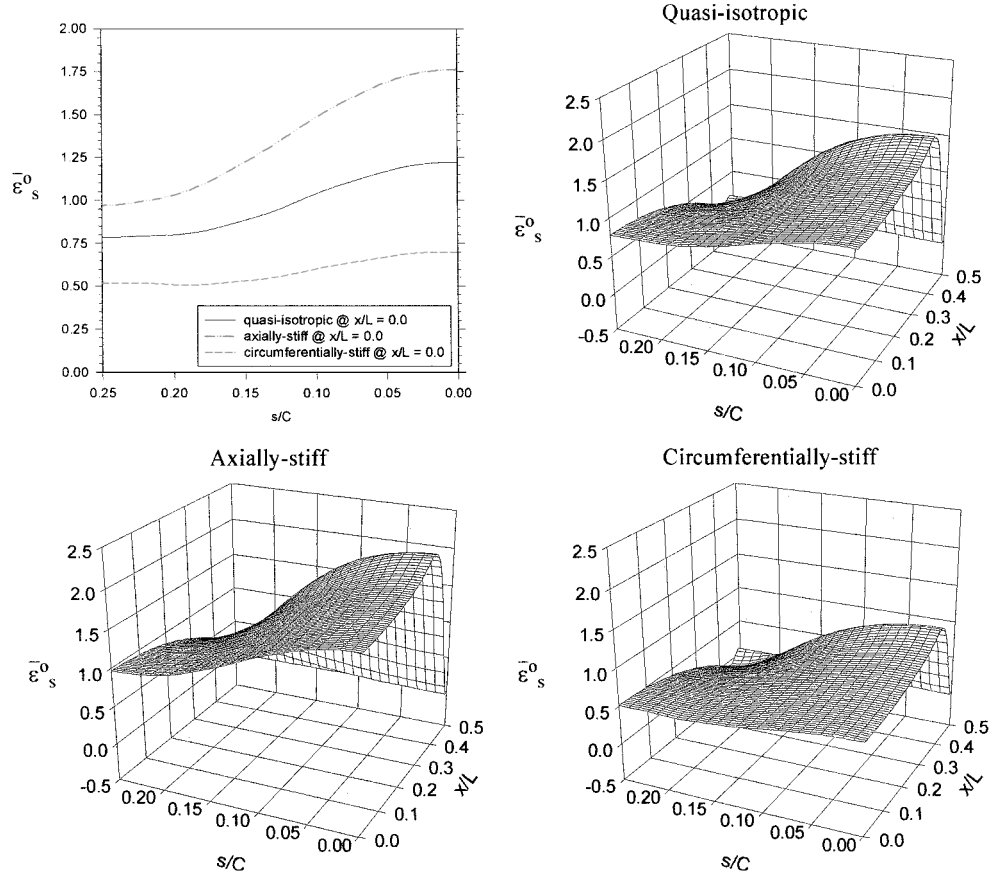

Fig. 4 Influence of orthotropy on the circumferential strain.

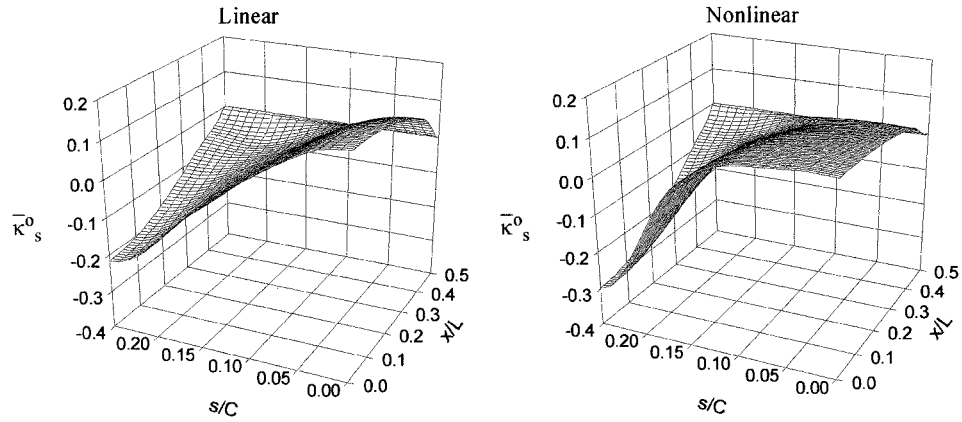

Fig. 5 Effect of geometric nonlinearities on the circumferential curvature.

are easily visible in Fig. 5. (The nondimensionalization factor is not relevant to the point to be made.) In the midspan region for the nonlinear analysis case, there is a significant flattening along the crown of the cylinder.

Failure Analysis

As the circumferential variation of cylinder response appears to depend on orthotropy as well as the varying curvature, it is difficult to pinpoint where failure will occur. The circumferential gradients in the response produce what could be considered locations of stress concentration for the noncircular geometry. These stress concentrations can be considered potential sites of failure initiation. For a circular geometry there would be no preferred circumferential location where failure would initiate. Rather, failure would be controlled by imperfections in the material caused by irregularities in the microstructure (broken fibers, wrinkled fibers, resin rich regions) or anamolies in the manufacturing process (ply gaps, ply overlaps, misaligned plys, etc.). Therefore, a consideration of failure is of value when studying elliptical cylinders. To that end, the Hashin and maximum stress failure criteria are used to evaluate failure initiation by considering geometrically linear and nonlinear analyses and axially stiff, quasi-isotropic, and circumferentially stiff cylinders. The failure criteria are used to assess the mode of failure (e.g., tensile or compressive fiber or matrix modes), the location of failure, and the pressure at failure. An interactive and a noninteractive criterion are considered for the purpose of studying the importance of stress interaction on failure predictions.

The interactive Hashin failure criterion[5] and the noninteractive maximum stress failure criterion[6] are both based on one-dimensional uniaxial and shear failure stresses, which are denoted as follows: σ_A^+ is the tensile failure stress in the fiber direction; σ_A^- the compressive failure stress in the fiber direction (absolute value); σ_T^+ the tensile failure stress transverse to the fiber direction; σ_T^- the compressive failure stress transverse to the fiber direction (absolute value); τ_T the transverse failure shear stress; and τ_A the axial failure shear stress. For graphite epoxy typical values of the failure stresses are as follows:

$$\sigma_A^+ = 1.482\ \text{GPa}, \qquad \sigma_T^+ = 50.0\ \text{MPa}, \qquad \tau_A = 100.0\ \text{MPa}$$
$$\sigma_A^- = 1.241\ \text{GPa}, \qquad \sigma_T^- = 200\ \text{MPa}, \qquad \tau_T = 100.0\ \text{MPa} \quad (10)$$

The failure modes of the Hashin criterion can be denoted as follows.

Tensile fiber mode ($\sigma_1 > 0$):

$$\left(\frac{\sigma_1}{\sigma_A^+}\right)^2 + \frac{1}{\tau_A^2}\left(\tau_{12}^2 + \tau_{13}^2\right) < 1 \quad (11)$$

Compressive fiber mode ($\sigma_1 < 0$):

$$\frac{-\sigma_1}{\sigma_A^-} < 1 \quad (12)$$

Tensile matrix mode ($\sigma_2 > 0$):

$$\left(\frac{\sigma_2}{\sigma_T^+}\right)^2 + \left(\frac{\tau_{23}}{\tau_T}\right)^2 + \frac{1}{\tau_A^2}\left(\tau_{12}^2 + \tau_{13}^2\right) < 1 \quad (13)$$

Compressive matrix mode ($\sigma_2 < 0$):

$$\frac{\sigma_2}{\sigma_T^-}\left[\left(\frac{\sigma_T^-}{2\tau_T}\right)^2 - 1\right] + \left(\frac{\sigma_2}{2\tau_T}\right)^2 + \left(\frac{\tau_{23}}{\tau_T}\right)^2 + \frac{1}{\tau_A^2}\left(\tau_{12}^2 + \tau_{13}^2\right) < 1 \quad (14)$$

In the preceding the subscripts 1, 2, and 3 on the stresses denote principal material coordinate system stresses, conventional notation. The normal stress σ_3 has been ignored because it is much smaller than the other two normal stresses, but the interlaminar shear stresses have been retained, as they could be important at the ends of the cylinder. The cylinder is assumed to be safe from failure if all four left-hand sides of Eqs. (11–14) are less than unity, and failure is assumed to have occurred if any one of the four left-hand sides equals unity. The failure modes of the maximum stress criterion can be denoted as follows.

Tensile modes ($\sigma_1, \sigma_2 > 0$):

$$\sigma_1/\sigma_A^+ < 1, \qquad \sigma_2/\sigma_T^+ < 1 \quad (15)$$

Compressive modes ($\sigma_1, \sigma_2 < 0$):

$$-\sigma_1/\sigma_A^- < 1, \qquad -\sigma_2/\sigma_T^- < 1 \quad (16)$$

Shear modes:

$$|\tau_{23}|/\tau_T < 1, \qquad |\tau_{13}|/\tau_A < 1, \qquad |\tau_{12}|/\tau_A < 1 \quad (17)$$

With this form of the failure criterion, the cylinder is assumed to be safe from failure if all seven of the left-hand sides of Eqs. (15–17) are less than unity, and failure is assumed to occur if any one of the seven left-hand sides equals unity.

To make use of either failure criterion, computation of the in-plane and interlaminar shear stresses in the principal material coordinate system is necessary. The computation of the in-plane stresses follows the standard approach of classical lamination theory. Computation of the interlaminar stresses is more complicated. Here, for the geometrically linear case the equilibrium equations of elasticity were integrated through the thickness of the cylinder wall, using the in-plane stresses derived from classical lamination theory as input, to obtain expressions for the through-thickness interlaminar stresses. For the geometrically nonlinear case the equilibrium equations of elasticity are quite complex compared to the linear case. Therefore, as an approximation, the interlaminar stresses for the geometrically nonlinear case were computed with the geometrically linear equations of elasticity, but using as input the in-plane stresses derived from classical lamination theory and including geometric nonlinearities. Background studies with circular cylinders, for which closed-form information is available, even for the nonlinear case, indicated

Table 1 Failure pressure, location, and mode for elliptical graphite-epoxy cylinders, geometrically linear and nonlinear analyses, two failure modes, two failure criteria

	Axially stiff		Quasi isotropic		Circumferentially stiff	
Case	Matrix	Fiber	Matrix	Fiber	Matrix	Fiber
Hashin						
Linear						
p_f, MPa	0.896	1.669	0.903	1.579	0.738	1.569
Location[a]	1/1 (+45)	9/2 (+45)	1/1 (+45)	8/2 (+45)	7/2 (90)	9/2 (+45)
s/C[b]	−0.07, +0.43	−0.08, +0.42	−0.07, +0.43	−0.07, +0.43	−0.25, +0.25	−0.06, +0.44
Mode	$+\sigma_2$	$-\sigma_1$	$+\sigma_2$	$-\sigma_1$	$+\sigma_2$	$-\sigma_1$
$\sigma_\kappa/\sigma_\varepsilon$	3.3/1	1.25/1	4/1	1.3/1	0.33/1	1.25/1
Nonlinear						
p_f, MPa	0.931	1.862	0.924	1.800	0.724	1.710
Location[a]	1/1 (+45)	9/2 (+45)	1/1 (+45)	8/2 (+45)	7/2 (90)	9/2 (+45)
s/C[b]	−0.09, +0.41	−0.11, +0.39	−0.10, +0.40	−0.10, +0.40	−0.25, +0.25	−0.26, +0.24
Mode	$+\sigma_2$	$-\sigma_1$	$+\sigma_2$	$-\sigma_1$	$+\sigma_2$	$+\sigma_1$
$\sigma_\kappa/\sigma_\varepsilon$	2.7/1	1.2/1	2.2/1	1.2/1	0.38/1	0.59/1
Maximum stress						
Linear						
p_f, MPa	0.938	1.669	0.938	1.579	0.738	1.569
Location[a]	1/1 (+45)	9/2 (+45)	1/1 (+45)	8/2 (+45)	7/2 (90)	9/2 (+45)
s/C[b]	−0.07, +0.43	−0.08, +0.42	−0.08, +0.42	−0.07, +0.43	−0.25, +0.25	−0.06, +0.44
Mode	$+\sigma_2$	$-\sigma_1$	$+\sigma_2$	$-\sigma_1$	$+\sigma_2$	$-\sigma_1$
$\sigma_\kappa/\sigma_\varepsilon$	3.3/1	1.25/1	2.86/1	1.3/1	0.33/1	1.25/1
Nonlinear						
p_f, MPa	0.965	1.862	0.958	1.800	0.724	1.834
Location[a]	1/1 (+45)	9/2 (+45)	1/1 (+45)	8/2 (+45)	7/2 (90)	9/2 (+45)
s/C[b]	−0.09, +0.41	−0.11, +0.39	−0.10, +0.40	−0.10, +0.40	−0.25, +0.25	−0.09, +0.41
Mode	$+\sigma_2$	$-\sigma_1$	$+\sigma_2$	$-\sigma_1$	$+\sigma_2$	$-\sigma_1$
$\sigma_\kappa/\sigma_\varepsilon$	2.3/1	1.2/1	2.2/1	1.2/1	0.38/1	1.28/1

[a]Location is given as layer number/interface, where 1 is the innermost layer and 1 denotes the inner and 2 the outer interface. The fiber direction of the layer is shown in parenthesis. 0° is the axial direction.
[b]Failures occur at $x/L = \pm 0.5$. Table is for $x/L = +0.5$: $s/C = 0$ is crown, $s/C = \pm 0.25$ are sides, C = circumference, and s = arclength measure.

that the through-thickness shear stresses computed by this approximate method agreed well with the stresses computed from a three-dimensional geometrically nonlinear finite element analysis. Furthermore, the background work indicated there was little difference between the through-thickness shear stresses computed by a three-dimensional geometrically linear analysis and the stresses computed by the same three-dimensional analysis but including geometric nonlinearities. In light of this background work, the approximate method was felt to be justified and certainly avoided the computations associated with a three-dimensional finite element analysis.

To compute the predicted failure pressure using the geometrically linear theory, the analyses were conducted using an internal pressure p_o of 0.690 MPa. The left-hand sides of the two failure criteria were then evaluated as a function of axial, circumferential, and through-thickness location within the cylinder wall. For each criterion the left-hand side that was closest to unity identified the failure location and failure mode. The pressure to cause failure was then determined by scaling the 0.690 MPa.

Two issues were immediately obvious from the geometrically linear failure analysis. First, the interlaminar stresses did not contribute to failure. The interlaminar stress components were much smaller than the in-plane components, and although the interlaminar failure stresses are small, the interlaminar components contributed little to the polynomials of the Hashin criterion and did not play a role in the maximum stress criterion. Second, both the Hashin and maximum stress criteria predicted first failure to be caused by in-plane matrix failure, i.e., matrix cracking, caused primarily by tensile stress perpendicular to the fibers, σ_2. Because the first matrix crack is not generally catastrophic, it was felt important to look at other failure conditions. Therefore, the pressure to cause first fiber failure was also computed. Ignored was any degradation in properties caused by further matrix failures occurring before fiber failure. This step was felt to be justified in light of the findings of a study,[7] which showed that for a pressurized quasi-isotropic elliptical cylinder the first fiber failure pressure was only 4% lower when material property degradation caused by matrix cracking was considered compared to the case of when it was ignored. Additionally, the location of failure was the same. Obviously, when pressure levels are high enough to produce significant amounts of fiber failure, further fiber failure predictions would depend on material degradation from previous fiber failures. However, because the mechanics of pressure containment, through the use of a liner or bladder, would have to be included to consider significant amounts of fiber failures, these pressures levels were not part of this study.

The upper quarter of Table 1 summarizes the findings of the geometrically linear analyses for the three laminates and the Hashin failure criterion. The table shows the failure pressure p_f, the failure location, the failure mode, and the ratio of the bending component of the stress at the failure location σ_κ to the in-plane component of stress there σ_ε. All failures are predicted to occur at two circumferential locations at each end of the cylinder, but Table 1 is for the end $x/L = +0.5$. As can be seen from the upper-left portion of the table, for the axially stiff cylinder matrix failure occurs at 0.896 MPa at the inner interface of the inner layer, i.e., loc = 1/1. In this particular instance the term *inner interface* is somewhat misleading because there is no interface between layers at the inner interface of layer 1, the inner +45-deg layer. The inner interface of layer 1 is the inner radial location of the cylinder wall. Circumferentially, failures occur about one-quarter of the distance from the crown, or keel, to the side ($s/C = -0.07$ and $s/C = +0.43$; see Fig. 1). Failure is caused by high tensile stresses perpendicular to the fibers in the plane of the layer, i.e., $+\sigma_2$. In this particular situation the component of σ_2 caused by bending effects is 3.3 times larger than the component of σ_2 caused by in-plane effects. Because failure occurs at the ends of the cylinder, large bending effects are to be expected as a result of the bending boundary layers there. For first fiber failure a pressure of almost twice the level is required, 1.669 MPa, and the mode of failure is fiber compression, i.e., $-\sigma_1$. The fiber failures occur in layer 9, the outer layer, at interface 2, the outer interface, i.e., the outer radius of the cylinder. This is a shift from the inside of the cylinder for matrix failure to the outside for fiber failure. The effect of bending is also reduced for the fiber failure. There are not failures at four symmetric s/C locations, e.g., $s/C = +0.07$ for matrix failure and $s/C = +0.08$ for fiber failure, because of the lack of material symmetry about the $s/C = 0$ location, i.e., $D_{16} \neq 0$ and $D_{26} \neq 0$. It was mentioned earlier that Figs. 2–5 showed the response for only

one octant of the cylinder strictly for convenience, not because of symmetry of response.

An a priori prediction of the circumferential location of failure would probably not include $s/C = -0.07$. Perhaps $s/C = 0$ or 0.25 would be the predicted location. It is felt the existence of circumferential displacements v^o, as shown in Fig. 2, is partially responsible for $s/C = 0$ or 0.25 not being the location. At the cylinder ends v^o is restrained to be zero, requiring an in-plane shear force resultant N_{xs} to achieve this. The transformation of the in-plane shear effect of N_{xs} into the principal material directions of the ± 45-deg layer leads directly to a stress component σ_2. This adds to the magnitude of σ_2 in these off-axis layers. Interestingly, N_{xs} is quite small at $s/C = 0, 0.25, 0.50$, and 0.75, the locations of geometric symmetry, and has extreme values roughly halfway between these circumferential locations. The increased value of N_{xs} away from the locations $s/C = 0, 0.25, 0.50$, and 0.75 is felt to be responsible for failure occuring away from the lines of geometric symmetry for this particular laminate.

The failure characteristics for the quasi-isotropic cylinder are similar to those for the axially stiff cylinder. The location of failure, the near doubling of the pressure to produce fiber failure, and the shift from an inner location for matrix failure to an outer location for fiber failure are all similar. The character of failure for the circumferentially stiff cylinder is somewhat different than the other two. The pressure to cause matrix failure is lower, and the failure locations are different. Matrix failure occurs in a layer outside the reference surface, layer 7, a 90-deg layer, at the sides of the cylinder $s/C = \pm 0.25$. At that location bending effects are not as important as in-plane effects, as indicated by the ratio of 0.33/1. An examination of the details of the deformations of the ellipse (not shown) reveals that at the crown and keel bending deformations are more pronounced than at the sides, and so the reduced role of bending effects at the sides of the cylinder is not surprising. Also, layer 7 is closer to the reference surface, a location where there are less bending effects than, say, at layer 9. For fiber failure for the circumferentially stiff cylinder, fiber compressive failure is again the mode, and this occurs at the outer radial location in layer 9, a $+45$-deg layer. The circumferential location is again about one-quarter of the distance from the crown to the side.

To compute the failure pressure using the geometrically nonlinear analysis, iteration was used, each iteration using a different internal pressure. The first step in the iteration process was the same as for the failure analysis for the geometrically linear case, namely, the analysis was conducted for a pressure of $p_o = 0.690$ MPa. Then, considering the maximum stress criterion as an example, the seven left-hand sides of the failure criterion were computed, and using $p_o = 0.690$ MPa the predicted failure pressure p_f was computed by scaling. The geometrically nonlinear analysis was conducted again using this predicted failure pressure, i.e., now p_o was the failure pressure predicted from the first step. The seven left-hand sides were again computed and were used to compute a new failure pressure. This procedure was repeated until the calculations were considered converged to the failure pressure. A similar iteration procedure was used for the Hashin criterion and the four left-hand sides in that criterion.

The second quarter of Table 1 summarizes the findings of the nonlinear analyses for the three laminates and the Hashin failure criterion. Considering the axially stiff case, it is seen that relative to the geometrically linear analyses geometric nonlinearities lead to slightly higher failure pressures, e.g., for matrix failure 0.931 MPa vs 0.896 MPa. As in the linear case, for matrix failure the tensile stress component σ_2 is responsible for failure, and for fiber failure a compressive σ_1 is responsible. For both matrix and fiber failure the through-thickness locations are identical to the linear case, and the circumferential location of failure moves just slightly away from the crown and keel. The ratio of the bending component of stress to the in-plane component is slightly lower for the geometrically nonlinear case. This is believed to be caused by the flattening effect caused by geometric nonlinearities. The comments for the axially stiff cylinder apply to the quasi-isotropic cylinder. Regarding the circumferentially stiff case, although geometric nonlinearities do not appear to significantly influence matrix failure, they do influence fiber failure predictions. The predicted mode changes from fiber compression for the linear analysis to fiber tension for the nonlinear analysis. Additionally, the location for the nonlinear analysis is near the sides as opposed to being in the crown and keel areas. The reason that the linear and nonlinear analyses do not agree for the fiber failure condition is that in the Hashin criterion for tensile fiber failure the shear stress τ_{12} is involved. For the nonlinear analysis the value of τ_{12} is greater than for the linear analysis, and the values of tensile σ_1 and τ_{12} near the sides of the cylinder outweigh the high values of fiber compression stress in the crown and keel regions.

The bottom half of Table 1 is a summary of using the maximum stress criterion to predict failure. An examination of the maximum stress criterion prediction reveals that many entries are similar, if not identical, to the Hashin criterion prediction. For the matrix failure the stress component σ_2 is so dominant that the Hashin criterion reduces, in effect, to the maximum stress criterion. The additional terms in the Hashin criterion have little influence. For fiber compression failure the Hashin criterion is identical to the maximum stress criterion so that the entries are the same in those cases. The primary difference occurs with fiber failure for the circumferentially stiff cylinder. Whereas with the nonlinear analysis the Hashin criterion predicts fiber tensile failure at the outer radial location near the sides, for the reasons just discussed, the maximum stress criterion prediction using the nonlinear analysis is similar to the linear analyses for both the Hashin and maximum stress criteria, namely, fiber compression at the outer radial location in the crown and keel regions. Overall, however, it appears that stress interaction is not overly important in the cases studied here.

Alternate View of Failure Predictions

With composite materials there is often scatter in the results from tests designed to determine failure stresses. Considering the failure stress of a composite material to be exactly a certain level is somewhat unrealistic. The scatter is caused by the aforementioned unpredictable irregularities in the microstructure of composites and possible anomalies in the manufacturing process. As a result, the location with the highest stress might not fail first. A slightly lower stress at another location, coupled with a microstructural irregularity, could lead to lower failure stress levels. To that end, the geometrically nonlinear failure analysis was used to compute the locations within the ellipse where the seven left-hand sides in the Hashin failure criterion were within 20% of the failure level, i.e., the left-hand sides of Eqs. (11–14) were in the range 0.80 to 1.00, with 1.00 corresponding to the cases discussed in Table 1 Figures 6–8 show these locations for the axially stiff, quasi-isotropic, and circumferentially stiff laminates, respectively. The location of first failure, i.e., matrix failure from Table 1, is also shown. The stresses were evaluated using nonlinear analysis at the matrix failure pressure p_f. In each figure a greatly distorted, and flattened, view of the crown section of the cylinder wall through the thickness from $-0.5 \le \zeta/H \le 0.5$ and around the circumference from $-0.25 \le s/C \le 0.25$ provides a visual display of the points within 20% of failure. All of these points are at the clamped end of the cylinder $x/L = 0.50$.

Referring to Fig. 6, as indicated in Table 1, the maximum left-hand side value, or initial failure point, for the axially stiff case is located at the first layer, a $+45$-deg layer, at the inner radial location of the cylinder at $s/C = -0.09$. Considering points where the left-hand side is less than 1.00, the points are dispersed circumferentially on both sides of the initial failure point in the first layer at the inner radial location. There are also points on both sides of the interface between the first and second layers. An alternative interpretation of the spatial distribution of the points is that if the pressure is increased beyond the value to predict first failure then there will be failure at another location. Further increases in pressure would lead to failure at other locations. It is felt that the geometric distribution of points in Fig. 6 would represent the progression of damage as the pressure increases beyond the value necessary to have the Hashin criterion to equal 1.00. If this interpretation is correct, then matrix cracking will accumulate in layer 1 at the inner radial location ($\zeta/H = -0.5$) in the range $-0.16 \le s/C \le 0$. There will also be cracking in layer 2 at the interface between the first and second layers. All of these failures would be caused by high values of σ_2. Though cracking

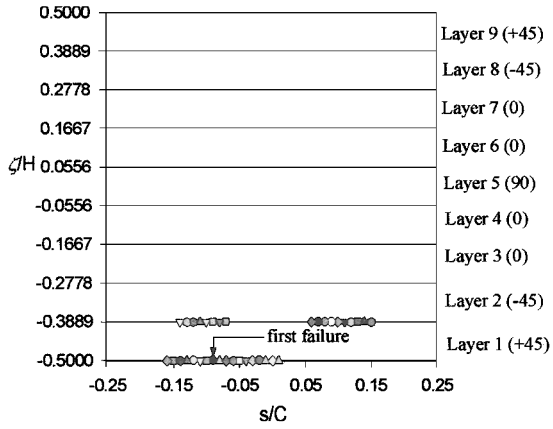

Fig. 6 Points within 20% of failure criterion equaling unity: axially stiff laminate, nonlinear analysis, $x/L = 0.5$, Hashin criterion.

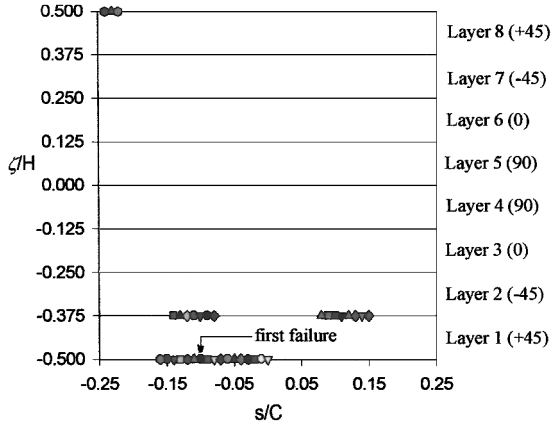

Fig. 7 Points within 20% of failure criterion equaling unity: quasi-isotropic laminate, nonlinear analysis, $x/L = 0.5$, Hashin criterion.

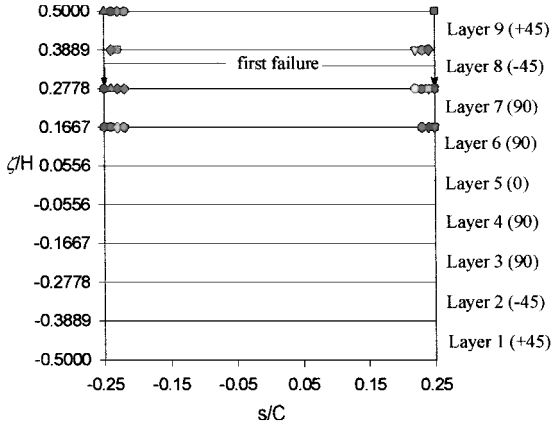

Fig. 8 Points within 20% of failure criterion equaling unity: circumferentially stiff laminate, nonlinear analysis, $x/L = 0.5$, Hashin criterion.

can begin at one interface or the other, because the stresses vary linearly through the thickness of a layer the crack probably would propogate entirely through the layer. Further increases in pressure would lead to more matrix cracking. Though in the strictest sense matrix cracking would lead to material degradation that would lead, in turn, to a redistribution of stresses, effects not included here, it is felt that Fig. 6 provides a reasonable indication of how matrix failure would progress.

Figure 7 shows similar matrix failure patterns occur for the quasi-isotropic case, although there are some matrix failures at outer radial locations (+45-deg layer). The circumferentially stiff case in Fig. 8 is different. Using the "progression of matrix cracking" interpretation for the locations of the points, it is seen matrix failure spreads from the two initial points at the sides and moves toward the crown ($s/C = 0$) along the interfaces between layers 6, 7, 8, and 9 and at the outer radial location.

Two issues must be kept in mind when considering Figs. 6–8. First, at some pressure level matrix failure will progress axially as well as circumferentially. Properly accounting for material degradation can show this happens before there is significantly more circumferential progression. Second, because the matrix failures at the locations shown in Fig. 6, for example, represents cracks through the entire thickness of the layers there are contiguous cracks through the two inner layers. The internal pressure is thus developing a leakage path through the cylinder the wall, an undesirable condition.

Conclusions

Presented has been a discussion of the response and initial failure of internally pressurized elliptical composite cylinders. The results demonstrate qualitatively and quantitatively the stress concentration effect of the noncircular geometry and the role of material orthotropy in governing cylinder response. Though a single degree of ellipticity has been studied, the effects discussed are felt to be general. It has been shown that for ellipses the displacement response is characterized by the existence of circumferential displacements and inward normal displacements at some circumferential locations. Compared to the axisymmetric response of a circular cylinder, there is considerable variation of the displacements, strains, and stresses components with circumferential location. The variation of these quantities is a function of the orthotropy of the cylinder, and it was shown that the circumferential strains at cylinder midspan varied less with circumferential location for the circumferentially stiff cylinder than for the axially stiff or quasi-isotropic cases. Thus material orthotropy can be used to some extent to mitigate, or counter, the effect of the noncircular geometry. It was also shown that the inclusion of geometric nonlinearities tends to flatten the crown. The study of failure revealed that the failure characteristics of the axially stiff and quasi-isotropic cylinders are similar and occur at similar failure pressures, whereas the failure characteristics of the circumferentially stiff cylinder are different than the other two cases and failure occurs at a lower pressure. In all cases the pressures to cause first fiber failure are about a factor of two greater than the pressures to cause first matrix cracking. Moreover, the maximum stress criterion generally predicts results similar to the Hashin criterion, indicating stress interaction effects are not important for first matrix failure and first fiber failure for the cases studied. Except for first matrix failure for the circumferentially stiff case, nonlinearities lead to slightly higher failure pressures and slightly different failure locations. For first matrix failure for the circumferentially stiff case, nonlinearities result in slightly lower failure pressures but the same failure location. Finally, the alternative view of failure suggests that a leakage path caused by matrix cracking can develop at specific and predictable locations as a result of the stress concentration effects associated with the noncircular geometry. Though small-scale elliptical cylinders have been considered, it is felt that the conclusions reached here can be extended to larger elliptical cylinders and, for example, oval cylinders. If, however, the radius of curvature varies rapidly over a small circumferential distance, such as with a square cross section with rounded corners, then an extension of the conclusions will most likely not apply.

Future activities should consider pressure levels to cause a significant amount of fiber failure and the acompanying degradation of material properties. This complicates the analysis considerably and dictates the use of an alternative analysis procedure, such as finite element analysis. Also, the influence of residual stresses caused by curing should be evaluated, particularly if the cylinders are to be used for cryogenic tankage, a situation where the temperature change relative to the cure temperature of the graphite epoxy is quite large.

Acknowledgments

The work reported on herein was supported by Grant NAG-1-1895 from the Mechanics and Durability Branch of the NASA Langley Research Center, Hampton, Virginia, to Virginia Polytechnic Institute and State University, Blacksburg, Virginia. The Virginia

Space Grant Consortium provided additional support. The authors sincerely appreciate the financial support from both sources. The NASA grant monitors were James H. Starnes Jr. and Damodar Ambur.

References

[1]Soldatos, K. P., "Mechanics of Cylindrical Shells with Noncircular Cross Section: A Survey," *Applied Mechanics Reviews*, Vol. 52, No. 8, 1999, pp. 237–274.

[2]Marguerre, K., "Stability of the Cylindrical Shell of Variable Curvature," NASA TM 1302, July 1951.

[3]IMSL MATH/Library User's Manual, IMSL, Inc., Houston, TX, 1987, pp. 660–671.

[4]Meyers, C. A., and Hyer, M. W., "Response of Elliptical Composite Cylinders to Axial Compressive Loading," *Mechanics of Composite Materials and Structures*, Vol. 6, No. 2, 1999, pp. 169–194.

[5]Hashin, Z., "Failure Criteria for Unidirectional Fiber Composites," *Journal of Applied Mechanics*, Vol. 47, No. 2, 1980, pp. 329–334.

[6]Hyer, M. W., *Stress Analysis of Fiber-Reinforced Composite Materials*, WCB/McGraw–Hill, New York, 1998, pp. 348–386.

[7]McMurray, J. M., and Hyer, M. W., "Progressive Failure Analysis of Internally Pressurized Elliptical Composite Cylinders," *Proceedings of the 15th Annual Technical Conference of the American Society for Composites*, edited by O. O. Ochoa, T. K. O'Brien, D. Lagoudas, and H. J. Sue, Technomic, Lancaster, PA, 2000, pp. 95–105.

A. M. Waas
Associate Editor